Contents lists available at ScienceDirect

Chemical Engineering Research and Design

journal homepage: www.elsevier.com/locate/cherd

Thermodynamic analysis of fuel oil blended stock (FOBS) model compound, *n*-eicosane to hydrogen via oxidative cracking

*Mei Lian Teo, Mazura Jusoh, Zaki Yamani Zakaria**

School of Chemical & Energy Engineering, Faculty of Engineering, Universiti Teknologi Malaysia, 81310 UTM Johor Bahru, Johor, Malaysia

ARTICLE INFO

Article history:
Received 16 August 2021
Received in revised form 30 November 2021
Accepted 14 December 2021
Available online 17 December 2021

Keywords:
Fuel oil blended stock
n-Eicosane, oxidative cracking
Hydrogen, light hydrocarbon

ABSTRACT

Petrochemical refineries worldwide experience a common problem: the accumulation of fuel oil blended stock (FOBS). FOBS are any leftover oil blended with other similar unfinished oils, to make a final refined product. FOBS are not only of no value, but also it triggers storage and environmental concern. One way to overcome this is to upgrade FOBS into higher value-added product through oxidative cracking process. In this study, FOBS potential as a feed was investigated to produce hydrogen by utilizing *n*-eicosane as the model compound. A thermodynamic equilibrium analysis based on the total Gibbs energy minimization method was performed for *n*-eicosane cracking to hydrogen in the presence of oxygen. The effects of different reactants ratio, temperature and pressure, were studied. Equilibrium product compositions of *n*-eicosane at temperatures of 573 K–1273 K, pressure of 0–20 bar, *n*-eicosane/oxygen ratios (EO) (0.5:0.5, 0.7:0.3, 0.8:0.2, 0.9:0.1, 0.95:0.05) were analysed. It was discovered that the main product of oxidative cracking is hydrogen and methane. Furthermore, the results showed that the optimum reactant ratio for hydrogen and methane production is EO ratio 0.95:0.05. A network of reaction mechanisms has been postulated to explain the overall complex reactions happening in the process.

1. Introduction

Crude oil is still responsible for 32% of the world energy supply and is expected to hold its position for the next decade (Hart et al., 2014; Wang et al., 2017). According to the International Energy Outlook 2016, the demand for fossil fuels in generating energy will still be prominent compared to other renewable energy in 2040 (Conti et al., 2016). The crude oil condensate and naphtha can be used after undergoing rigorous processing in a refinery to produce numerous types of derivatives, which involve several complicated processes. However, there will be situation where undesired by-products are formed, could not be blended with other feedstock, because the amount is too much or it has extreme unfavourable properties, and eventually stored in a designated storage tank as fuel oil blended stock (FOBS). Although the operation department of the refineries will do their very best to utilize all available precious feed stock and side-products, some still end up as FOBS. FOBS is defined as any leftover oil or product that is blended with other similar unfinished oils, to make a final refined product, but often it is regarded as undesired products due to its difficulty to be further processed. After certain amount of time, FOBS can partially or into certain extend with time transformed to sludge which will then be tougher to handle. Upon its transformation to sludge, refinery operation will regard it as scheduled waste and the disposal will require tedious care and humongous cost. The refinery is capable of paying for the disposal cost, but this will be only a fast and temporary but unsustainable solution for the refinery. In addition, the scheduled waste will end up somewhere at a scheduled waste treatment facility and involve either further processing, landfilling or incinerated depending on the severity of the hazardous compound it contains. That is why it is imperative to urgently seek a way to reverse this scenario and investigate alternatives to convert FOBS into value-added products, which can increase profitability of the business and minimize environmental concerns.

FOBS contained fuel oils that consist of a diverse range of hydrocarbons obtained through crude oil refining (Laffon, 2014). It has larger carbon content than gasoline and naphtha, ranging between 20 and 70

* *Corresponding author.*
E-mail address: zakiyamani@utm.my (Z.Y. Zakaria).
https://doi.org/10.1016/j.cherd.2021.12.020

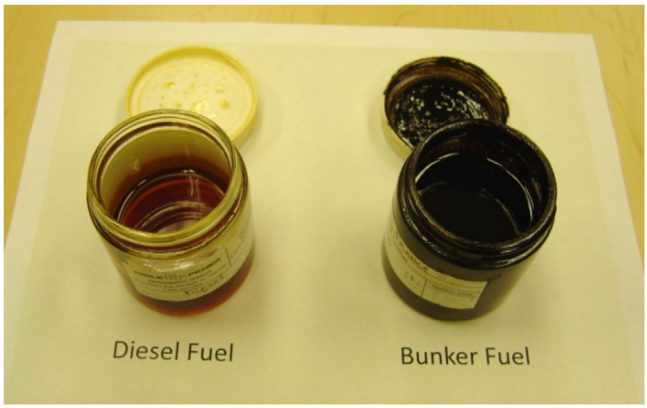

Fig. 1 – Colour difference of Fuel Oil No.6 (Bunker Fuel) with Diesel Fuel (Agency, 2021).

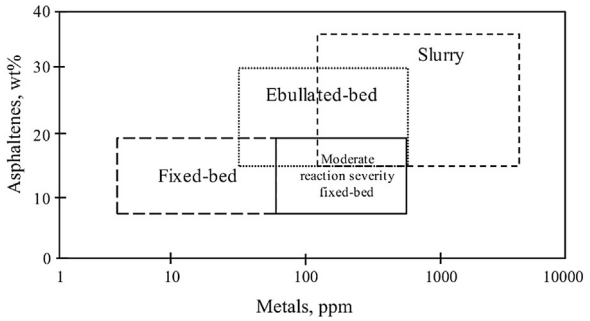

Fig. 2 – Selection of hydrocracking technologies based on the contents of the feedstock (Angeles et al., 2014).

carbon atoms. The two main types of FOBS are distillate fuel oils and residual fuel oils. Heavy Fuel Oil (HFO), also known as Fuel Oil No. 6 or Bunker Fuel, is one of the most abundant FOBS from petroleum refinery. It is a residual fuel oil from petroleum refineries that is generally blended with additional components to improve the oil quality. Normally, cutter stock or blend components are blended with this residual from oil refineries to bring down the high viscosity of the HFO, bringing it to certain specifications. It is hoped that through this process, the economic value of the FOBS produced increases. Unfortunately, most of the time, this is not the case. For instance, not only refineries throughout the world is having problem dealing with HFO, but the HFO at power generation plants also led to the environmental and financial crisis that the government has to endure (Al-Malack et al., 2016).

Since FOBS (that contained HFO) has become more abundant with time, it is necessary to pursue a solution to overcome all the problematic issues arising from it. This attracted some research where HFO were upgraded to form lighter fuel that produces cleaner energy on burning (Ghashghaee, 2017; Kar et al., 2018). Such upgrading process of fuel oil offered modern approach to re-purpose the HFO in a more sustainable method and reduces environmental problems caused by HFO. The effort is spot on with time as it was introduced amidst the scarcity of natural oil and gas era as well as the strengthening control of environmental laws and regulations.

In the American Society for Testing and Materials (ASTM) D396 standard, fuel oils from FOBS are divided into six groups based on boiling point, composition and purpose (Perry et al., 1998). A noticeable difference that could be observed between HFO (Fuel Oil No. 6) with other fuel oil is their colour. Fuel oil No. 1 to No. 4 could be colourless to brown. In contrast, the colour of HFO with a tar-like appearance is black. The darker colour of HFO reveals that it is thicker, with a higher viscosity than other fuel oil. Apart from that, HFO also has a high specific gravity compared to other lighter fuels (Schmidt, 1985). A comparison of the colour difference of HFO (Bunker Fuel) with diesel fuel is shown in Fig. 1 (Agency, 2021). The main components of HFO are saturates, aromatics, resins, and asphaltenes (Stratiev et al., 2016; Zhao et al., 2019). The molecular weight of HFO is generally affected by the composition of asphaltenes and aromatics which are the high molecular weight compounds. The presence of asphaltenes contributes to the dark colour of HFO and makes HFO a dense material (Demirbas et al., 2016). The presence of aromatics as a stable compound has increased the difficulty in directly burning HFO as a fuel (Garaniya et al., 2011). The sources of fuel oil affect the compositions of each component in HFO.

Generally, the preferred transformation process of FOBS is through thermochemical conversion processes that can be categorised into thermal cracking, hydrocracking and catalytic cracking (Taghili et al., 2020). The four main factors that impact the process are catalyst development, the origin of FOBS, engineering decisions in process planning, and economic considerations (Akhavan et al., 2014). Since the 1900s, numerous studies had been conducted to investigate the cracking of various hydrocarbons. The thermolysis of higher molecular weight of n-paraffins, including n-eicosane in the vapour-phase, proved that 1-alkenes could be formed as the main product (Zhou et al., 1987).

Thermal cracking, also known as pyrolysis, is a simple process involving burning fuel to supply heat to a temperature higher than 350 °C in the cracking reactor to produce a wide range of liquid and gases products. The burning of fuel outside the reactor releases a large amount of carbon dioxide into the atmosphere. Visbreaking and coking processes are examples of thermal cracking (Sviridenko et al., 2020). Visbreaking, also known as mild cracking, is used to reduce the viscosity of FOBS, while coking is a cracking process that involves longer residence time. In most researches, cracking is only valid for a low conversion of feedstocks (Jiang et al., 2019; Zhu et al., 2014). The cracking temperature was controlled at a suitable range to ensure only primary and secondary cracking occurred. Thermal cracking at lower temperature encourages the production of liquid fuels, while a higher temperature promotes olefins production (Ghashghaee and Shirvani, 2018).

Catalytic cracking has been the centre of attention in recent years. A more significant amount of olefins with higher market demand and lesser paraffins could be formed as the products. Common catalysts employed include zeolite ZSM-5 (Elordi et al., 2011; Safari et al., 2020, 2019), Molybdenum oxide (Taghili et al., 2020), Li/MgO (Boyadjian et al., 2010), etc. Hydrocracking could be further classified as thermal hydrocracking and catalytic hydrocracking. The co-feeding of hydrogen with feedstocks in hydrocracking could promote the production of products that have higher hydrogen to carbon ratio. Hydrogen provides better control of the cracking process and reduces the amount of coke formed in the reactor (Hasanova et al., 2019). For hydrocracking reaction, the available type of reactors includes fixed-bed, slurry-phase, ebullated-bed, and others. The criteria for selecting hydrocracking technologies are summarised in Fig. 2 (Angeles et al., 2014).

Recently, the addition of atmospheric oxygen to assist the upgrading process of FOBS has been introduced as it helps reduce the emission of harmful pollutants such as carbon dioxide. The use of oxygen would increase carbon monoxide production instead of carbon dioxide in the selectivity of CO_x formation. The advantages of using oxygen in the upgrading process also include increasing the production of light fractions and reducing coke formation in the reactor (McDermott et al., 2020). Nevertheless, the amount of oxygen fed into the cracking process is kept low, that is less than 8 wt% in the reactants for process safety purpose (Shvets et al., 2017). Production of oxygen-containing compounds such as oxides could be detected while oxygenated products such as alcohol could be neglected as the small amount of oxygen supplied is insufficient for the complete oxidation of feedstocks.

Table 1 summarises previous researches on FOBS and hydrocarbon upgrading. The final products produced at the end of the upgrading process depend on the reactants, reaction parameters and technology used. Heavy fuel oil with a lower commercial value undergoes the cracking process to produce smaller hydrocarbon molecules with a higher retail value that meet the market demand. Due to the differences in compositions of FOBS from different resources, the upgrading process of the FOBS may produce various products depending on the reactant used. Based on SARA analysis (saturates, asphaltenes, resins, aromatics in heavy crude oil), HFO contains a high percentage of sat-

Table 1 – Summary on upgrading technology.

Process	Reaction Parameters	Feed stocks	Products	Refs.
Thermal Cracking	Temperature range at 800 K–2200 K, pressure at 5, 30, 150 and 760 Torr	n-Decane with Argon	Paraffins, olefins, benzene, hydrogen gas, diene, alkynes	(Zeng et al., 2014)
Thermal Cracking	Temperature range at 150 °C–450 °C, reactor pressurized at 0.69 MPa	Heavy oils	Naphtha, distillates, gas oil, vacuum residue, coke	(Rueda-Velásquez and Gray, 2017)
Thermal Cracking	Temperature range at 750–1430 K, pressure at 0.0066, 0.039, 0.197 and 1 atm	n-Dodecane with Argon	Paraffins, olefins, benzene, hydrogen gas, diene, alkynes	(Zeng et al., 2018)
Thermal Cracking	Temperature range at 450 °C–730 °C, pressure at 3MPa	n-Dodecane	450 °C–530 °C: Paraffins, olefins, 0.3% cycloalkane; 530 °C–600 °C: cycloalkene, MAHs; > 600 °C: PAHs, coke	(Zhang et al., 2018)
Thermal Cracking	Temperature range at 580 K–940 K, pressure at 4–6 MPa	n-Decane	Paraffins, olefins, hydrogen gas(Result only valid for conversion up to 13%)	(Jiang et al., 2019)
Thermal and catalytic cracking with low-cost catalyst	Temperature range at 240 °C–290 °C	Heavy crude oil	Paraffins, Olefins, aromatic, cycloalkane	(Kar et al., 2018)
Catalytic cracking with alumina nanoparticles	Temperature range at 400 °C–420 °C	Athabasca vacuum residue	Asphaltene, maltene, toluene insoluble	(Eshraghian and Husein, 2018)
Visbreaking with MoO3/γ-Al2O3 nanocatalyst	Temperature range at 250 °C–350 °C, atmospheric pressure	Extra heavy oil	Gaseous products, liquid products	(Taghili et al., 2020)
Thermal and catalytic cracking with NiCr/WC catalyst	Temperature range at 350 °C–450 °C, pressure at 6 MPa	Heavy crude oil	Gaseous products, liquid products, coke	(Sviridenko et al., 2020)
Catalytic cracking with equilibrium catalyst or hydrothermally deactivated catalysts	Temperature range at 450 °C–500 °C, atmospheric pressure	Bio-oil and *n*-eicosane	Gaseous hydrocarbon, coke, CO, CO_2, oxygenates, water	(Shimada et al., 2018)
Hydrocracking with dispersed catalyst	Different range of condition (depend on the catalyst used)	Heavy oil with hydrogen	Gaseous products, liquid (oil fractions), coke	(Angeles et al., 2014)
Hydrocracking with halloysite modified	Temperature at 430 °C, pressure at 0.5–6 MPa	Heavy fuel oil hydrogen	Gasoline (paraffins, iso-paraffins, unsaturated, naphthenes, aromatics), Diesel, Coke	(Hasanova et al., 2019)
Thermal cracking with addition of oxygen	Temperature range at 430–450 °C, pressure at 3 atm	Black oil fuel and oxygen	Paraffins, olefins, aromatic, Low coke (almost no coke).	(Shvets et al., 2016)
Thermal cracking with addition of oxygen	Temperature range 430–460 °C, pressure at 2–8 atm	Heavy oil residues and oxygen	Paraffins, olefins, aromatic hydrocarbon	(Shvets et al., 2017)
Oxidative catalytic cracking with ZSM-5 zeolite	Temperature at 550 °C, atmospheric pressure	Heavy oil residues and oxygen	Naphtha, kerosene, Diesel	(Safari et al., 2020)
Oxidative catalytic cracking with hexagonal boron nitride	Temperature range 1023 K–1173 K, atmospheric pressure	n-butane and oxygen	CH_4, CO, CO_2, C_2H_4, C_2H_6, C_3H_6, C_4H_8	(McDermott et al., 2020)
Oxidative Dehydrogenation	Temperature range 475–575 °C	Ethane and oxygen	H_2, CH_4, H_2O, CO, CO_2, C_2H_4 and C_2H_2	(Dar et al., 2021)

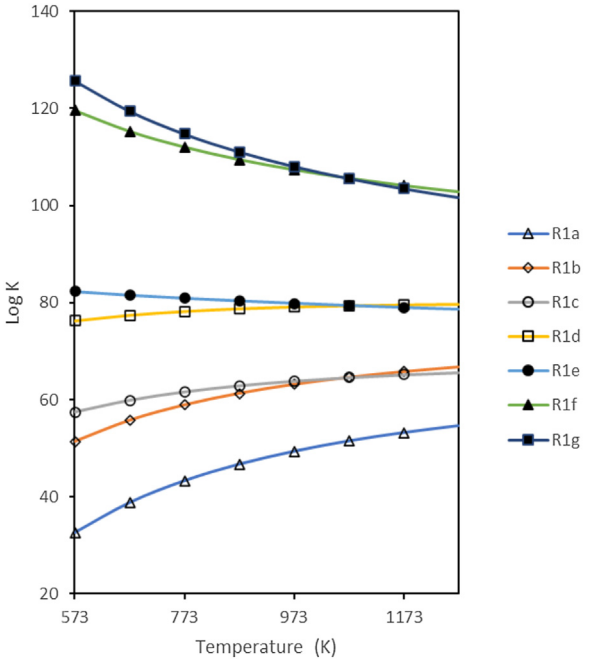

Fig. 3 – Equilibrium constant of R1a-R1g in the oxidative cracking of n-eicosane with oxygen at 1 bar and different temperature.

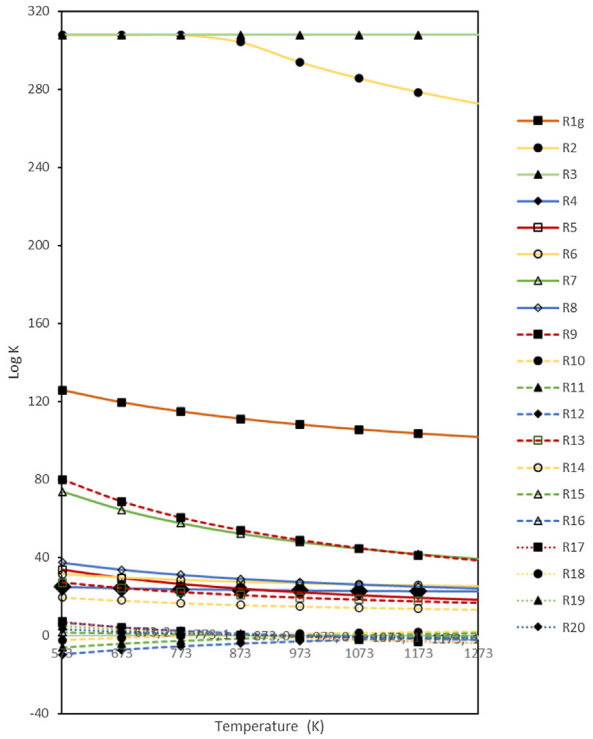

Fig. 4 – Equilibrium constant of R1g, R2-R20 in the oxidative cracking of *n*-eicosane with oxygen at 1 bar and different temperature.

urates and aromatics, including different kinds of paraffin (Garaniya et al., 2011; Stratiev et al., 2016). The sample of HFO collected from Mexican reported 11.5 wt.% of saturates, 18.2 wt.% of aromatics, 47.0 wt.% of resins and 23.3 wt.% of asphaltenes (Alonso-Ramírez et al., 2018). On the other hand, the HFO in Pei's study shows the highest percentage in asphaltene (Pei et al., 2020). At present, it is impossible to find out the exact composition of each component in FOBS as it is a mixture of various compounds. All of these resulted in a complicated transformation process to upgrade FOBS.

With only a tiny amount of non-hydrocarbon in HFO, it is reasonable to neglect them in the simulation of the upgrading process as it brings a negligible effect on the characteristics of HFO (Jiang et al., 2013). With adequate calibration, it was revealed that suitable combinations of n-paraffins could be used to present the viscous behaviour of HFO (Dante et al., 2006). Pure hydrocarbons were chosen to represent heavy fuel oil in previous studies due to the high percentages of hydrocarbon in the fuel oil (Dante et al., 2006; Jiang et al., 2013). In view of this, the present thermodynamic modelling study focuses on oxygenated cracking of *n*-eicosane, which is part of HFO, as a model compound for FOBS. *n*-Eicosane has 20 carbon atoms and is within the range of HFO (n-C20 to n-C70). It is a suitable model compound to initiate deeper investigation of this study. Nevertheless, limited researches were conducted to investigate the cracking of heavy fuel oil with oxygen to initiate the upgrading process. Most of it focused on cracking hydrocarbon with less than 10 carbons or heavy oils with various compositions. No similar research had been conducted on oxygenated cracking with n-eicosane as the surrogate fuel. This thermodynamics modelling will provide simulation process that helps deal with the complexity of a design process by providing a better understanding of the process of *n*-eicosane oxidative cracking to hydrogen and light hydrocarbons.

Possible products formed under oxidative cracking of *n*-eicosane were identified under various reaction parameters such as temperature and reactant ratio by applying the total Gibbs energy minimization method. Number of moles of products formed were analysed under equilibrium conversion. The reactions that may take place in this process were identified based on the feasibility of the process. The effect of both pressure and temperature on products formed were analysed. The usage of ambient oxygen aims to open the chances of low-cost reactant in enhancing the cracking process. Thus, the problem of increasing FOBS production in the petrochemical refineries could be further reduced by converting FOBS into more valuable products.

2. Method

2.1. *Model compound of FOBS*

The simulation investigation was carried out using a model compound of FOBS due to the complexity of FOBS composition. Hydrocarbon is generally chosen and the selected hydrocarbon should reflect the major hydrocarbon types present in commercial fuel, including n-alkanes, iso-alkanes, cycloalkanes, and aromatics (Wu et al., 2019a, 2019b). For simplification, most researchers only used one or two compounds to represent FOBS in studies. Difference characteristics of the compound such as molecular weight and structure, density and availability should be considered wisely to ensure the selected compound can really represent the FOBS. The n-eicosane, as known as icosane, was selected as the model compound of HFO, consequently representing FOBS in this study. This is because *n*-eicosane is proven that it could be used as one of the multi-component model compounds of HFO (Sun et al., 2019). *n*-Eicosane, *n*-20 was also used to represent the HFO in the catalytic cracking of HFO with bio-oil (Shimada et al., 2018). In addition n-eicosane, $C_{20}H_{42}$ is a straight-chain alkane that consists of 20 carbon atoms. It falls under the acceptable carbon range of HFO. It is a stable hydrocarbon with van der Waals forces. In addition, it is insoluble in water, with a solubility of 1.2114×10^{-4} ppm in water (Yaws and Gabbula, 2003). The n-eicosane appears as a colourless or white solid, with a melting point range between 35.1 °C–38 °C (Nabil and Khodadadi, 2013). With a low phase change-point between 36 °C–38 °C, it has been used as a phase change material (PCM) in storing heat energy (Zhang et al., 2020). Due to its high flash point at 212 °F (Program, n.d.), n-eicosane is less flammable and inefficient to be used as a fuel. The other properties of n-eicosane are summarised in Table 2.

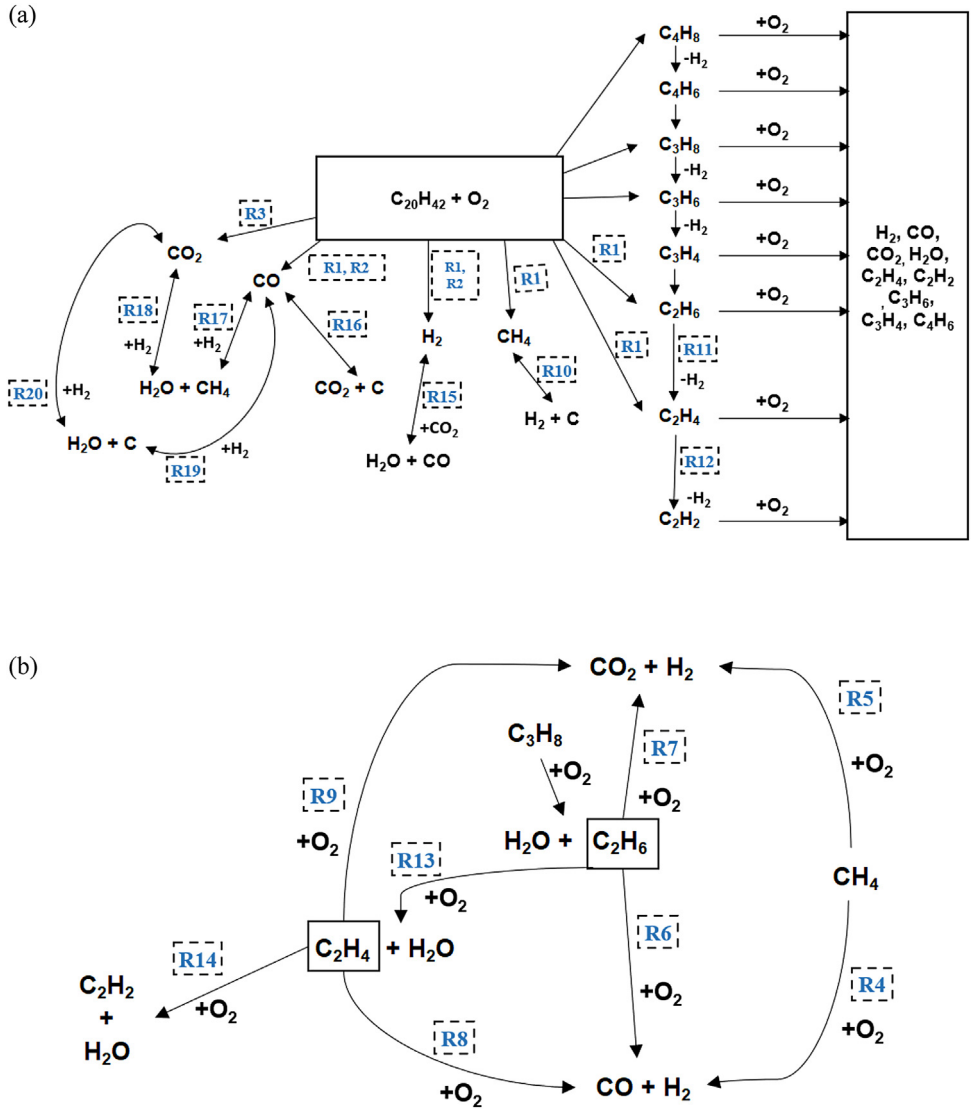

Fig. 5 – (a) Overall reaction network (b) Additional reaction network based on products formed in the oxidative cracking of n-eicosane with oxygen at 1 bar.

Table 2 – Properties of *n*-eicosane [43].

Properties	Value
CAS Registry no.	112-95-8
Molecular weight	282.553 g/gmol
Boiling point	616.93 K
Critical temperature	767.04 K
Critical pressure	10.40 bar
Refractive index, n_D at 20 °C	1.4425
Gibbs energy of formation at 298 K	115.66 kJ/mol
Thermal conductivity of gas	0.005 W/(mK) at 298 K 0.0036 W/(mK) at T_{min} = 250 K 0.0363 W/(mK) at T_{max} = 1000 K
Viscosity of gas	34.641 μP at 298 K 29.138 μP at T_{min} = 250 K 115.29 μP at T_{max} = 1000 K
Surface tension	10.54 dyne/cm at 538.32 K
Solubility parameter at 36 °C	15.77 $(J/cm^3)^{1/2}$
Dipole moment (D)	0
Van der Waals' area at 36 °C	2.854×10^{10} cm^2/mol

2.2. *Thermodynamic analysis*

The thermodynamic analysis of oxidative cracking of n-eicosane with oxygen was performed using HSC Chemistry version 11.0 software based on the minimization method of the total Gibbs energy (Roine, 1999). All chemical species involved were considered when the system reached equilibrium at constant temperature and pressure. The equilibrium rate constants for all possible reactions were determined and the equilibrium compositions of each species were calculated when the Gibbs energy of the system reached its minimum. The total Gibbs Free energy of a system with more than one phase and components is shown in the equation below (Henderson et al., 2020).

$$nG = \sum_{i=1}^{S}\sum_{j=1}^{Mp}(n_{ij}G_{ij}) \quad (1)$$

where M_p and S are the number of phases in the system and the number of species in the system, respectively. The minimization of total Gibbs Free energy in the gas phase is shown in Eq.2 when considering solid carbon formation in this process (Zeng et al., 2010).

$$G^t = \sum_{i=1}^{N-1} n_i\left(\Delta G^0_{fi} + RT\ln\frac{f_i}{f^0_i}\right) + n_c\Delta G^0_{fc} \quad (2)$$

where ΔG_{fi}^{0} is the standard Gibbs function of each species i and ΔG_{fc}^{0} is the standard Gibbs function of carbon, f_i is the fugacity of species i.

The species considered in this study were n-eicosane and oxygen as the reactants. Ambient air is supplied to the reactor to supply the oxygen stream. Since air mainly consists of nitrogen and oxygen, the nitrogen supply could act as an unreactive medium, providing stabilization on the reaction temperature and enhancing the energy efficiency of the process (Shrestha et al., 2017; Zhong et al., 2021). Therefore, nitrogen supply is omitted as a reactant in the simulation study as it remains unreacted in the reactor. Meanwhile, the reaction products were hydrogen, carbon (coke), methane, water, carbon monoxide, carbon dioxide, ethane, ethene, acetylene, propyne, allene, propane, propene, 1,3-butadiene and butene. The possible products formed were identified through literature reviews from prior studies as listed in Table 1. Heavier compounds are not detected as it is subjected to secondary reactions in the reactor until equilibrium is reached. The Gibbs software is used to find the most stable species combination at the equilibrium phase. Therefore, only small compounds as listed had been detected at minimum total Gibbs energy. Other compounds such as aromatic compounds are not detected because the reaction conditions used are inadequate for their production. It only happens when there is severe cracking in a high-temperature setting (Zhang et al., 2018).

The outlet composition of the products was assumed to be in equilibrium at the exit of the reactor. For gas-phase reaction equilibrium, a mixture of ideal gases was assumed. Solid carbon is the only species that exist in the solid phase. The total number of mol of reactant input was kept at 1 kmol. The three main thermodynamic parameters: temperature, feed ratio and pressure, are considered in this study. The operating temperature was kept in the range of 573 K–1273 K while the ratios of n-eicosane to oxygen (EO) were 0.5:0.5, 0.7:0.3, 0.8:0.2, 0.9:0.1 and 0.95:0.05. In all conditions, the pressure was kept at 1 bar. Complete conversion of n-eicosane was recorded in all considered reaction parameters, indicating the feasibility of the oxidative cracking of n-eicosane with oxygen. After getting the optimum ratio for product conversion, the pressure and temperature effect on the oxidative cracking process was assessed using contour graphs, where the pressure ranges from 0 to 20 bars. The overall oxidative cracking of FOBS with oxygen is a complex reaction that involves multiple side reactions such as partial oxidation, dehydrogenation, oxidative dehydrogenation, methanation and water gas-shift reaction. The simulation performed in this study represents the oxidative cracking process in the cracking reactor in a plant. *n*-Eicosane is fed into the reactor, followed by the ambient air that provides oxygen. The reactor should be equipped with a suitable temperature controller and thermocouple for the experimental study to ensure the oxidative cracking process occurs at the required temperature. Control valves are employed to control the pressure of the reactor. The reactor should contain a safety valve for emergency shutdown. The reaction network of the whole process was proposed based on former postulations (Dar et al., 2021; Hosseinpour et al., 2019; Li and Zhao, 2015; Zeng et al., 2018).

2.3. *Equilirium constant, K*

The Gibbs free energy change of reactions (ΔG_r^0) and enthalpy change of reactions (ΔH_r^0) at 298.15 K are obtained from HSC Chemistry Software Database. The equilibrium constant, K of all possible reactions is calculated using Eqs. 3 and 4.

$$K' = e^{-\frac{\Delta G_r^0}{RT}} \tag{3}$$

$$ln\,K = -\frac{\Delta H_r^0}{R}\left(\frac{1}{T} - \frac{1}{T'}\right) + \ln K' \tag{4}$$

where R is 8.314 $Jmol^{-1}\,K^{-1}$, K' is the equilibrium rate constant of reaction at 298.15 K and T' is reference temperature at 2981.5 K. The effect of temperature on the equilibrium constant of all possible reactions is analysed.

3. Results and discussion

3.1. *Ln K vs T and possible reactions*

All possible reactions that may occur in the oxidative cracking of *n*-eicosane for the formation of main products were identified. There is a total of 20 reactions proposed in this process (Table 4). The first initial reaction that occurs in this process is R1 and 7 possible reactions that might occur from R1 oxidative cracking of *n*-eicosane are listed as R1a to R1g in Table 3. The equilibrium constant, K calculated could use to determine the extent of each reaction. From Fig. 3, Ln K values of all R1 reactions are bigger than zero within the temperature range in this study (573 K–1273 K). R1a to R1d is endothermic and spontaneous, while R1e to R1g is exothermic and spontaneous at all temperature. All R1 are product-favoured reaction at the studied temperature. The thermal cracking of pure hydrocarbon without oxygen is an endothermic process as heat energy is required to break down the chemical bond to form smaller components (Jin et al., 2017; Safari et al., 2020; Shrestha et al., 2017). The fuel is burned outside the reactor to supply heat energy to the reactor. A high reaction temperature is needed in the traditional thermal cracking, causing an increased emission of greenhouse gases such as carbon dioxide into the atmosphere.

On the other hand, oxidative cracking with the addition of oxygen could overcome these problems. The cracking with induced oxygen could occur in an autothermic mode due to the exothermic route provided in the presence of oxygen. A primary exothermic reaction is beneficial to the overall process as the heat release enables energy conservation inside the reactor, the reaction mixture in the reactor could be raised to a higher temperature in a shorter time (Magomedov et al., 2014), reducing the energy input required to the reactor at the same time (McDermott et al., 2020). Thus, a smaller amount of fuel is burned outside the reactor in the oxidative cracking than the thermal cracking. This helps reduce the cost of fuel consumption and the release of CO_2 from the burning of fuel. Moreover, the use of oxygen as a free radical initiator significantly reduced the activation energy needed in bond cleavage of the free radical mechanism in the cracking of n-eicosane. The addition of oxygen also promotes other exothermic side reactions such as oxidative dehydrogenation that increase the yield of olefins than the conventional thermal cracking. In addition, the formation of coke as a side product could be reduced as oxygen works as a decoking agent. Oxygen-induced cracking also reduces the reactor's size and enhances the conversion of reactants compared to thermal cracking. Thus, the oxidative cracking of *n*-eicosane is employed to replace the conventional thermal cracking in this study.

Table 3 – Reactions in the oxidative cracking of *n*-eicosane with oxygen.

Reaction	Type of Reaction	Equation	ΔH_{298} (kJ/mol)	ΔG_{298} (kJ/mol)
R1a	Oxidative Cracking of n-eicosane with O_2	$C_{20}H_{42}(g) + O_2(g) \rightarrow H_2(g) + 2\ CO(g) + CH_4(g) + C_2H_6(g) + 7.5\ C_2H_4(g)$	468.493	37.308
R1b	Oxidative Cracking of n-eicosane with O_2	$C_{20}H_{42}(g) + 1.5\ O_2(g) \rightarrow 2\ H_2(g) + 3\ CO(g) + CH_4(g) + C_2H_6(g) + 7\ C_2H_4(g)$	331.751	−134.051
R1c	Oxidative Cracking of n-eicosane with O_2	$C_{20}H_{42}(g) + 1.5\ O_2(g) \rightarrow H_2(g) + 3\ CO(g) + CH_4(g) + 2\ C_2H_6(g) + 6\ C_2H_4(g)$	194.667	−235.240
R1d	Oxidative Cracking of n-eicosane with O_2	$C_{20}H_{42}(g) + 2\ O_2(g) \rightarrow 2\ H_2(g) + 4\ CO(g) + 2\ CH_4(g) + C_2H_6(g) + 6\ C_2H_4(g)$	94.210	−390.119
R1e	Oxidative Cracking of n-eicosane with O_2	$C_{20}H_{42}(g) + 2\ O_2(g) \rightarrow H_2(g) + 4\ CO(g) + 2\ CH_4(g) + 2\ C_2H_6(g) + 5\ C_2H_4(g)$	−42.874	−491.308
R1f	Oxidative Cracking of n-eicosane with O_2	$C_{20}H_{42}(g) + 3\ O_2(g) \rightarrow 3\ H_2(g) + 6\ CO(g) + 2\ CH_4(g) + 2\ C_2H_6(g) + 4\ C_2H_4(g)$	−316.357	−834.025
R1g	Oxidative Cracking of n-eicosane with O_2	$C_{20}H_{42}(g) + 3\ O_2(g) \rightarrow 2\ H_2(g) + 6\ CO(g) + 2\ CH_4(g) + 3\ C_2H_6(g) + 3\ C_2H_4(g)$	−453.441	−935.213

Table 4 – Side Reactions in the oxidative cracking of *n*-eicosane with oxygen.

Reaction	Type of Reaction	Equation	ΔH_{298} (kJ/mol)	ΔG_{298} (kJ/mol)
R2	Partial oxidation of n-eicosane with O_2	$C_{20}H_{42}(g) + 10\ O_2(g) \rightarrow 21\ H_2(g) + 20\ CO(g)$	−1754.966	−2861.248
R3	Partial oxidation of n-eicosane with O_2	$C_{20}H_{42}(g) + 20\ O_2(g) \rightarrow 21\ H_2(g) + 20\ CO_2(g)$	−7414.245	−8004.930
R4	Partial oxidation of methane with O_2	$2\ CH_4(g) + O_2(g) \rightarrow 4\ H_2(g) + 2\ CO(g)$	−71.883	−173.299
R5	Partial oxidation of methane with O_2	$CH_4(g) + O_2(g) \rightarrow 2\ H_2(g) + CO_2(g)$	−318.905	−343.833
R6	Partial oxidation of ethane with O_2	$C_2H_6(g) + O_2(g) \rightarrow 3\ H_2(g) + 2\ CO(g)$	−136.398	−241.528
R7	Partial oxidation of ethane with O_2	$C_2H_6(g) + 2\ O_2(g) \rightarrow 3\ H_2(g) + 2\ CO_2(g)$	−702.326	−755.896
R8	Partial oxidation of ethene with O_2	$C_2H_4(g) + O_2(g) \rightarrow 2\ H_2(g) + 2\ CO(g)$	−273.483	−342.717
R9	Partial oxidation of ethene with O_2	$C_2H_4(g) + 2\ O_2(g) \rightarrow 2\ H_2(g) + 2\ CO_2(g)$	−839.410	−857.085
R10	Methane decomposition	$CH_4(g) \leftrightarrow 2H_2(g) + C(s)$	74.600	50.530
R11	Dehydrogenation of ethane	$C_2H_6(g) \leftrightarrow C_2H_4(g) + H_2(g)$	137.084	101.189
R12	Dehydrogenation of ethane	$C_2H_4(g) \leftrightarrow C_2H_2(g) + H_2(g)$	175.000	141.521
R13	Oxidative dehydrogenation of ethane	$2\ C_2H_6(g) + O_2(g) \rightarrow 2\ C_2H_4(g) + 2\ H_2O(g)$	−209.484	−254.786
R14	Oxidative dehydrogenation of ethene	$2\ C_2H_4(g) + O_2(g) \rightarrow 2\ C_2H_2(g) + 2\ H_2O(g)$	−133.652	−174.121
R15	Water gas shift reaction	$CO(g) + H_2O(g) \leftrightarrow H_2(g) + CO_2(g)$	−41.138	−28.602
R16	Boudouard Reaction	$2CO(g) \leftrightarrow CO_2(g) + C(s)$	−172.423	−120.004
R17	Methanation	$CO(g) + 3\ H_2(g) \leftrightarrow CH_4(g) + H_2O(g)$	−205.885	−141.932
R18	Methanation	$CO_2(g) + 4\ H_2(g) \leftrightarrow CH_4(g) + 2\ H_2O(g)$	−164.747	−113.330
R19	Reduction of CO	$H_2(g) + CO(g) \leftrightarrow H_2O(g) + C(s)$	−131.285	−91.402
R20	Reduction of CO_2	$CO_2(g) + 2H_2(g) \leftrightarrow 2H_2O(g) + C(s)$	−90.147	−62.800

It can be observed that from R1a to R1g, the enthalpy of reaction become more negative as the reaction become more exothermic with the increase in stoichiometry coefficients of oxygen in the reaction. Since the reaction from R1e to R1g is exothermic with negative ΔG_r^0 value, the higher log K value in Fig. 3 shows that the reaction is more feasible as a spontaneous reaction. Therefore, R1g is selected to represent the cracking of n-eicosane with O_2 as the exothermic nature of this reaction could compensate the endothermic nature of the cracking process, reducing external energy needed to supply to the reactor.

Based on Fig. 4, partial oxidation of hydrocarbon (R2 to R9) is exothermic and spontaneous, with the feasibility of reaction decrease with increasing temperature. Only R3 shows constant Ln K value among the partial oxidation processes. The extremely high Ln K value in R2 and R3 shows that both reactions go to completion in the selected temperature range. For R10, it is an endothermic reaction with increasing Ln K value. Equilibrium is limited at lower temperature, the formation of carbon is feasible at temperature higher than 873.15 K. Dehydrogenation (R11 and R12) is endothermic reaction, the equilibrium is limited for R12 while for R11, reaction only occur at temperature higher than 1073.15 K. Oxidative dehydrogenation (R13 and R14) is exothermic reaction and equilibrium unlimited. The water gas shift reaction (R15) and Bourdouard reaction (R16) are exothermic where reactions are feasible at temperature lower than 1073.15 K and 873.15 K, respectively. Both methanation (R17 and R18) are exothermic, more likely to occur in lower temperature and equilibrium limitation at higher temperature. Also, both R19 and R20 are exothermic that favour the production of carbon at lower temperature.

3.2. *Reaction network*

The reaction network based on the products formed is shown in Fig. 5. Both exothermic and endothermic reactions that occurred are illustrated together to provide a better overview of the process. The oxidative cracking process begins with the main reaction (R1) that required high energy to crack the large hydrocarbon, *n*-eicosane into smaller hydrocarbon. With the use of oxygen, it can be observed that products that contain oxygen atoms are formed in this oxidative cracking process. As shown in the first step of Fig. 5(a), other than the production of smaller alkanes and alkenes, the reactions between *n*-eicosane and oxygen (R1-R3) also produce CO, CO_2 and hydrogen as the first products from both oxidative cracking (R1) and partial oxidation processes (R2, R3).

During the oxidative cracking process, a free radical mechanism that initials by the C—C bond homolytic scission occurs: $-R \rightarrow 2R\cdot$. The presence of oxygen would increase the rate of the cracking by enhancing the cleavage in C–H bond to produce hydroperoxyl radical and alkyl radical simultaneously:

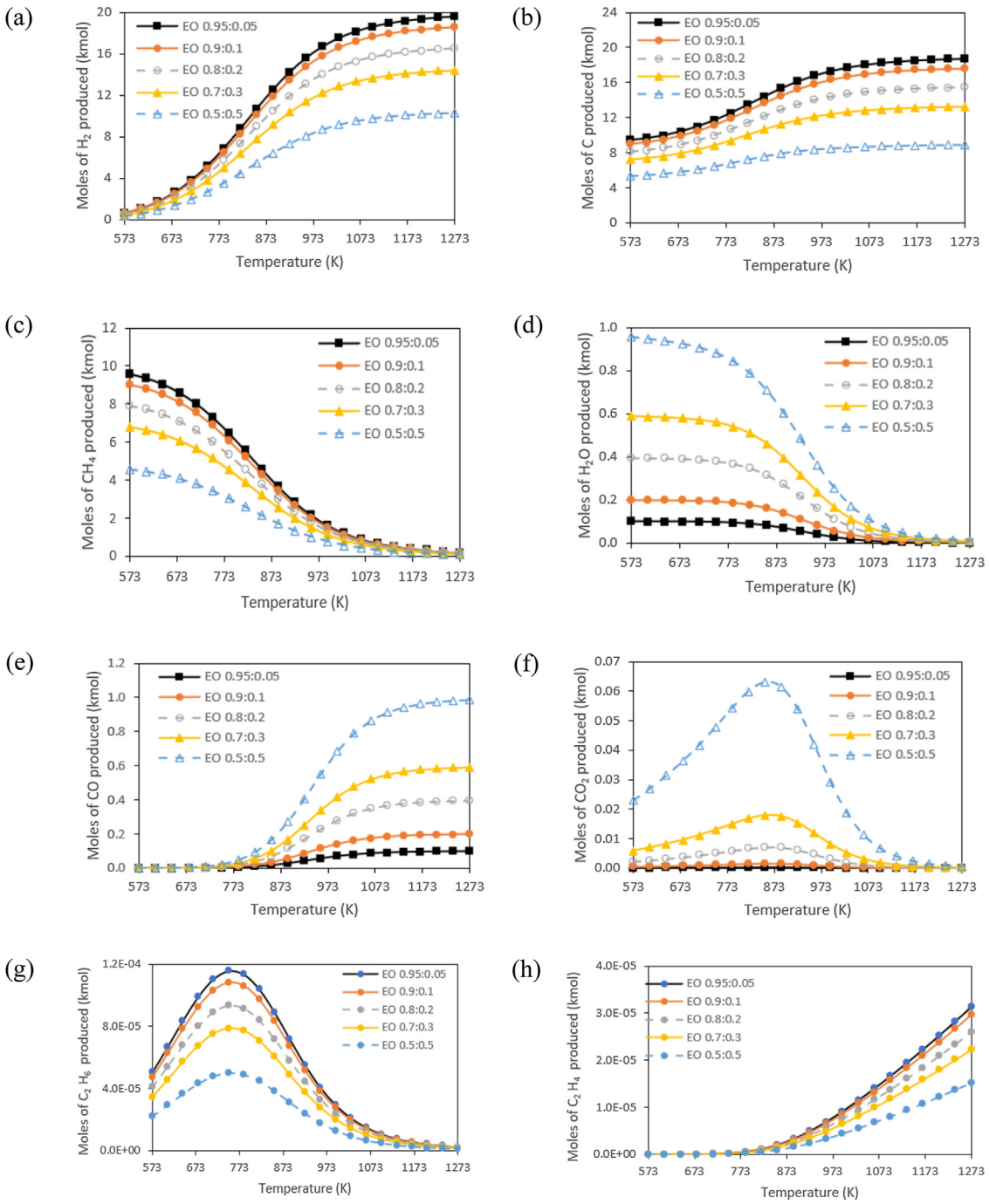

Fig. 6 – Moles of (a) H_2 (b) C (c) CH_4 (d) H_2O (e) CO and (f) CO_2 (g) C_2H_6 (h) C_2H_4 produced in the oxidative cracking of *n*-eicosane with oxygen at 1 bar.

$C_{20}H_{41} - H + O_2 \rightarrow C_{20}H_{41}\cdot + HOO\cdot$. The free radicals then undergo β-scission to form alkene and smaller radicals: $R\cdot \rightarrow R + R\cdot$. Meanwhile, H-abstraction (hydrogen transfer reaction) via unimolecular reaction leads to the formation of alkene while H-abstraction via bimolecular reaction leads to the formation of alkane: $R + R\cdot \rightarrow R + R\cdot$. H-abstraction in $HOO\cdot$ and hydrocarbon would form radicals and hydrogen peroxide, which would eventually form radical and water: $0.5\,H_2O_2 \rightarrow OH\cdot\ H_2O + R\cdot$. Other than oxygen-containing radicals that had been mentioned, other radicals that might be formed in this series of reactions are ·H, $\cdot CH_3$, $\cdot C_2H_3$, $\cdot C_2H_5$, $\cdot C_3H_7$, $\cdot C_4H_7$, $\cdot C_4H_9$, $\cdot C_5H_{11}$, $\cdot C_3H_3$ and $\cdot aC_3H_5$. The radicals' reaction is terminated by the combination of radicals, forming alkane and alkene that include C_4H_8(g), C_3H_8(g), C_3H_6(g), C_2H_6(g) and C_2H_4(g). After that, each of the first products undergoes secondary reactions (R4-R20), respectively until an equilibrium condition is achieved. Pyrolysis of smaller components (R10) and side reactions (R4-R9, R11-R20) occur subsequently. The hydrocarbons would undergo further decomposition in the next chain reaction—for example, the formation of ethane and ethene from butane.

Methanation occurs when CO (R17) and CO_2 (R18) react with hydrogen, respectively. The conversion of CO to CO_2 and solid carbon (R16) happens through the Boudouard Reaction. Besides, the hydrogen would also react with CO_2 (R15) in the water gas shift reaction. All smaller hydrocarbons react with oxygen (R4-R9), respectively, in partial oxidation to produce hydrogen, CO and CO_2. The exothermic oxidative dehydrogenation (R13-R14) and endothermic dehydrogenation (R11-R12) that involves the hydrogen abstraction from

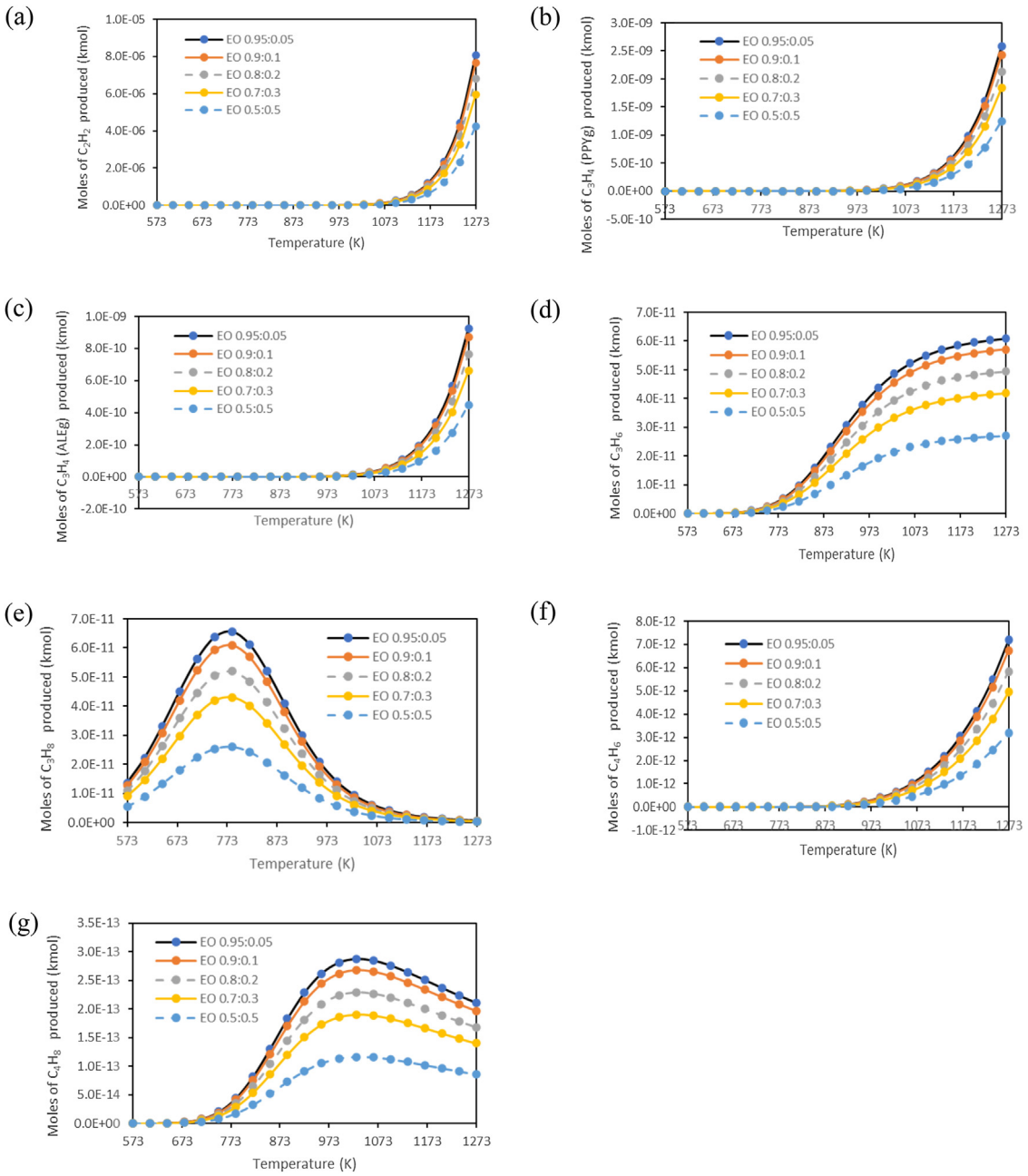

Fig. 7 – Moles of (a) C_2H_2 (b) C_3H_4 (Propyne) (c) C_3H_4 (Allene) (d) C_3H_6 (e) C_3H_8 (f) C_4H_6 (g) C_4H_8 produced in the oxidative cracking of *n*-eicosane with oxygen at 1 bar.

hydrocarbon occurs in both alkane and alkene. Water could be produced via the oxidative dehydrogenation process (R13-R14). The formation of diene and alkyne occurred via the secondary cracking of alkene through H-abstraction. For instance, $C_4H_8 \rightarrow \cdot C_4H_7 \rightarrow C_4H_6$. On the other hand, alkyne could be formed through the successive decay of alkenyl (Zeng et al., 2018). That is $C_2H_4 \rightarrow \cdot C_2H_3 \rightarrow C_2H_2$ in endothermic dehydrogenation. Reduction of both CO (R19) and CO_2 (R20) lead to the formation of water and carbon. In this study, there are no aromatic or branched olefins recorded in the product equilibrium composition. Only linear alpha-olefin is found in the outlet composition. In short, a series of chain reactions occur during the oxidative cracking process.

In the oxidative cracking process, the main products formed are H_2(g), C(s), CH_4(g), H_2O(g), CO(g), CO_2(g), C_2H_6(g), C_2H_4(g) and C_2H_2(g) while the minor products formed are C_3H_4(g), C_3H_8(g), C_3H_6(g), C_4H_6(g), C_4H_8(g), C_4H_{10}(g). Among the main products, hydrogen recorded the highest value of production compared to others. In addition, the result of thermodynamics analysis showed that there is the production of oxygenated products such as formaldehyde (CH_2O), methanol (CH_3OH) and acetaldehyde (CH_3CHO). The formation of oxygenates is due to the complete oxidation of hydrocarbons or radicals. For instance, the oxidation of C_1 radicals to produce formaldehyde. The oxygenates would undergo H-abstraction to produce smaller radicals and atoms. However, due to the small amount of oxygen supplied in the reactants at all EO ratios, the yield of oxygenated products is insignificant and could be neglected. Therefore, the production of oxygenated products was omitted in the current research. The production trends of each product are discussed in next section. Besides, it is found that the percentage of oxygen conversion is almost 100% for all EO ratios.

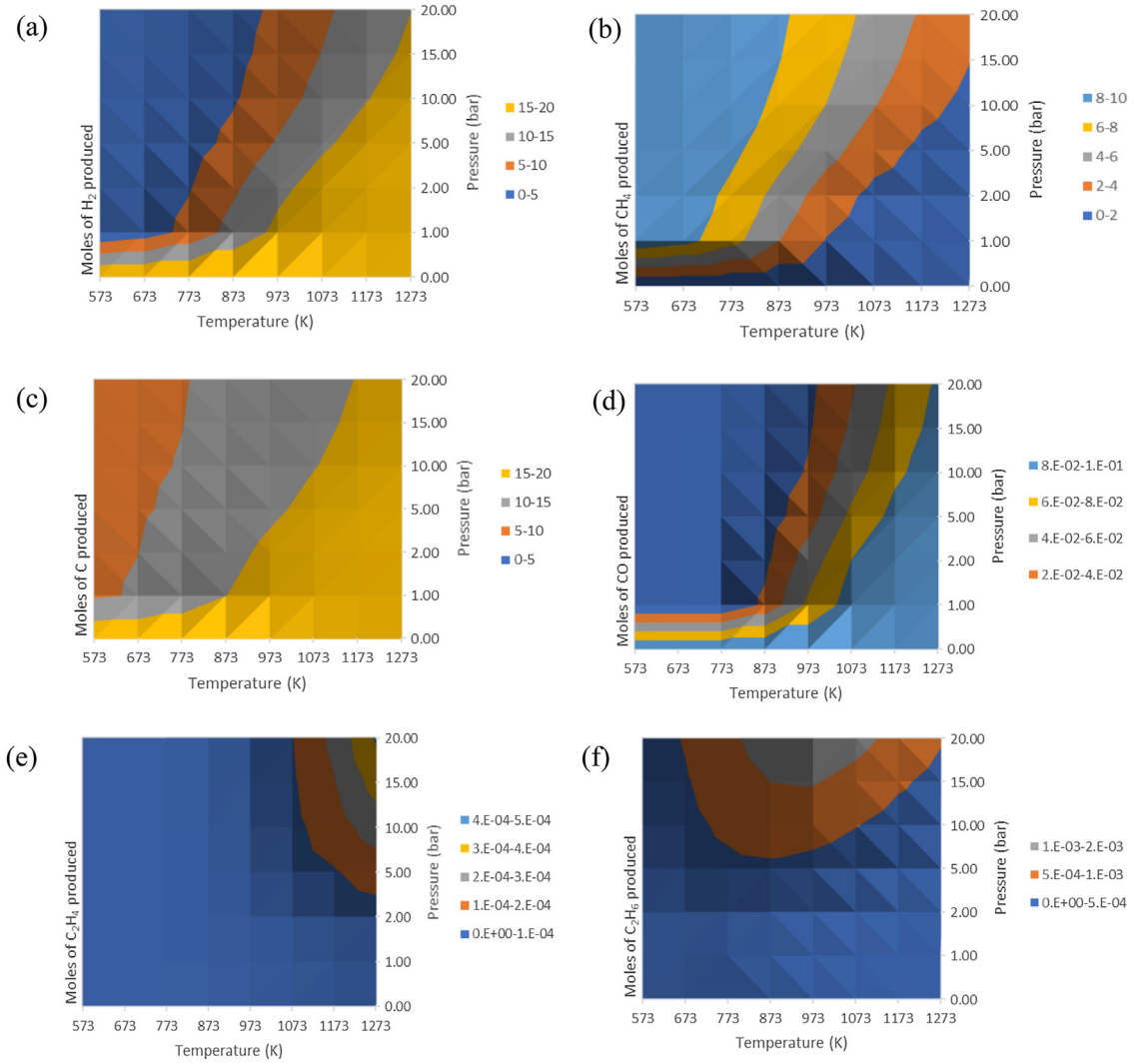

Fig. 8 – Moles of (a) H_2 (b) CH_4 (c) C (d) CO (e) C_2H_4 (f) C_2H_6 produced in the oxidative cracking of *n*-eicosane with oxygen at different temperature (573 K–1273 K) and pressure (0–20 bar).

3.3. *Effect of temperature on oxidative cracking of n-eicosane with oxygen at 1 bar*

Fig. 6(a) illustrates the hydrogen production in the oxidative cracking of *n*-eicosane with oxygen at 1 bar. Currently, steam reforming is the most dominant process for hydrogen production in the industry as it brings more advantages than other hydrogen production processes. However, the oxidative cracking in this study also has its advantages. A large amount of heat release with the addition of oxygen in upgrading could also reduce the viscosity of HFO (Pei et al., 2020). Since lesser energy is required during the upgrading process, it promotes hydrogen production with lower energy consumption. Moreover, the partial oxidation occurred is a considerably faster process than steam reforming and is able to compact the reactor (He et al., 2013). Therefore, it requires a smaller reactor vessel to operate.

The number of moles of hydrogen produced increases with the increase of the reaction temperature. The highest number of moles of hydrogen produced can be observed in the highest EO ratio, which is 0.95:0.05 whereas the lowest EO ratio 0.5:0.5 produced the lowest amount of hydrogen. At all EO ratios, the production of hydrogen showed a rapid increase from 573 K to 853 K. After 853 K, the increment in hydrogen production almost remains stable, showing that higher-temperature conditions above 1273 K will no longer promote higher production of hydrogen. The rapid increase in the production of hydrogen in the early stage is mainly caused by R1, R2 and R3. The high yield of hydrogen in this process is beneficial as it has a variety of usage (Abdalla et al., 2018).

Fig. 6(b) illustrates the carbon production for oxidative cracking of n-eicosane with oxygen at 1 bar. The high EO ratio and high temperature favour the production of carbon. More carbon is produced in the highest EO ratio 0.95:0.05, due to the availability of more carbon in the reactant, while the lowest carbon is produced in the lowest EO ratio 0.5:0.5. The production of carbon can be explained via R10, R16, R19 and R20. R10 favours carbon formation at higher temperature. Inversely, R16, R19 and R20 favours carbon formation at lower temperature. Carbon production is undesired in a catalytic reaction as it will deactivate the catalyst (Eshraghian and Husein, 2018). However, in this study, no catalyst is used; therefore the oxidative cracking process is less affected by the production of carbon (petcoke). The petcoke formation is not totally unpleasant as it has a high calorific value, around 37 MJ/kg (Lee and Choi, 2000), making it suitable as an alternative for fuel supply (Pei et al., 2020). Moreover, due to its high carbon content, it could be sell for the production of various products, especially in aluminium, power, storage, cement, steel and other industry (Manasrah, 2018). On the flip side, the high

formation of carbon might cause the accumulation of carbon and clog the processes after some time (Angeles et al., 2014). This should be taken into consideration in the engineering design process of the reactor. Proper handling is needed to avoid unpleasant circumstance.

Fig. 6(c) shows the methane production for the oxidative cracking of *n*-eicosane with oxygen at 1 bar. Methane has the highest yield among the light hydrocarbon formation in the cracking process (Shvets et al., 2017). Compared to hydrogen production, methane formation could be an undesirable product since it competes with hydrogen for the hydrogen atom. Methane production should be significantly minimised to optimise the fuel efficiency for hydrogen generation. However, methane formation is critical as it acts as the predecessor to the production of hydrogen. The formation of methane is higher at lower temperatures and it decreases gradually with the increase of reaction temperature. This is due to the exothermicity of methanation via R17 and R18. Similar to carbon formation, more methane is produced in a higher EO ratio due to the presence of more carbon in the reactant.

Fig. 6(d) shows the water production for the oxidative cracking of *n*-eicosane with oxygen at 1 bar. When temperature increase, the formation of water decrease. A low EO ratio promotes higher water formation due to the presence of more oxygen in the feed, especially at low temperatures. The formation of water in high EO ratio is smaller and steadier. Even though water is an unwanted product in this process, the methanation of CO_x in R17 and R18 has contributed to similar production trend for methane and water.

Fig. 6(e) illustrates the carbon monoxide production for oxidative cracking of *n*-eicosane with oxygen at 1 bar. When the temperature of reaction increases, the moles of CO produced increase. The rising trend of CO production at higher temperature is due to the presence of oxygen that promotes partial oxidation of *n*-eicosane. This situation is similar to the oxidative cracking of naphthenic and aromatic hydrocarbons (Zhu et al., 2006). Therefore, it is observed that at the lowest EO ratio 0.5:0.5, the presence of more oxygen promotes towards highest production of CO. The use of oxygen induces the cracking of *n*-eicosane by enhancing the selectivity of CO_x in products formed compare to traditional pyrolysis. The production of CO is desired as it is valuable petrochemical feedstock that can generate other compounds, for instance to produce synthetic fuels via Fischer–Tropsch synthesis (Mehariya et al., 2020).

Fig. 6(f) illustrates the carbon dioxide production for the oxidative cracking of *n*-eicosane with oxygen at 1 bar. The formation of CO_2 is sturdier at a high EO ratio. A lower EO ratio promotes the formation of CO_2 compared to a high EO. The amount of CO_2 produced at low EO ratio increase slowly until it achieves the maximum amount at temperatures 800 K–900 K. Although the small amount of CO_2 created may appear to be an environmental disadvantage, the amount of CO_2 produced in oxidative cracking is lower than the direct usage of FOBS during combustion. The proposed upgrading process also provides an alternative to disposing of the growing amount of residual fuel oil produced worldwide. Generally, the yield of CO_2 produced in oxidative cracking is lower than CO compared to conventional cracking (Liu et al., 2004). A lower amount of CO_2 production is advantageous as it helps to reduce the release of greenhouse gases into the atmosphere. Therefore, the use of limited oxygen in this cracking is believed to create a more environmentally friendly process than the traditional cracking process. Nevertheless, further studies are required to reduce the CO_2 production in fossil-based reactants during hydrogen production.

Fig. 6(g) shows the ethane production in the oxidative cracking of *n*-eicosane with oxygen at 1 bar. The production of ethane is mainly triggered by reaction R1. The number of moles of ethane increases from 573 K to a maximum point around 753 K. At higher temperatures, the amount of ethane decreases due to reaction R11. A higher EO ratio promotes higher ethane production due to the availability of carbon in the reactants.

Fig. 6(h) illustrates the ethylene production in the oxidative cracking of *n*-eicosane with oxygen at 1 bar. It is detected that ethylene conversion increase with the increase in temperature in all EO ratio. Higher EO ratio recorded higher ethylene yield due to the higher number of carbons in reactant at R1. The oxidative cracking in R1 is mainly responsible for ethylene production before side reactions occur.

By comparing Figs. 6(b) and 6(c), it can be observed that the formation of methane is preferred as the primary carbon product at a lower temperature compared to carbon. Therefore, it can deduced that methane formation is most prevailing before reaching certain oxidative cracking point at a higher temperature (Henderson et al., 2020).

When the yield of ethane starts to drop from its maximum point around 750 K, it is recorded that there is an increasing trend in the production of ethylene as shown in Fig. 6(h). This situation is mainly attributed to the R11 that converts ethane to ethylene. In other words, with the increase in temperature, the production of 1-olefin is higher than *n*-paraffins with more than one carbon. The β-scission of radicals occur to promote the production of ethylene when the temperature increases (Li and Zhao, 2015; Liu et al., 2019, 2016).

Other than the main products, side products formed in this process include lower number hydrocarbons such as acetylene, propyne, allene, propane, propene, 1,3-butadiene and butene. The production of triple bond hydrocarbon: acetylene, propyne and allene are in trace amount as it highly depends on the secondary cracking of olefins. The acetylene production in the oxidative cracking of *n*-eicosane with oxygen at 1 bar is shown in Fig. 7(a). At all EO ratios, it can be observed that the production of acetylene at low temperature is in trace amount, and the yield increases gradually after 1073 K. The production of acetylene recorded its highest value at higher EO, EO ratio 0.95:0.05 while at the lowest EO, the yield of acetylene is considerably low. The production of acetylene is triggered by R12 and R14. It could be shown that the production of acetylene is mainly dependent on the availability of ethene. Hence, the production trend of acetylene is similar to the production trend of ethene. The yields of both products increase when the temperature increase.

There are two C_3H_4 products that could be formed in this process, namely propyne and allene. Figs. 7(b) and 7(c) illustrate the propyne and allene production in the oxidative cracking of *n*-eicosane with oxygen at 1 bar, respectively. The production trends of both substances are similar to that in acetylene. The yield of C_3H_4 shows a significant increment after 1073 K in all EO ratios. The highest number of moles of C_3H_4 are recorded in the highest temperature. Higher EO ratio, 0.95:0.05 promote the production of C_3H_4. As shown in Fig. 5(a), the dehydrogenation and oxidative dehydrogenation of propene lead to the production of C_3H_4. The formation of propene increases when the temperature increases, which would lead to the formation of C_3H_4 in a series of chain reactions.

Fig. 7(d) shows the propene production in the oxidative cracking of *n*-eicosane with oxygen at 1 bar. The number of moles of propene produced rise with the temperature. The highest propene production could be detected in a high EO ratio, whereas a low EO ratio 0.5:0.5 showed the lowest production with the smallest increment in the overall trend. According to Fig. 5(a), propene is produced from the secondary cracking of propane. Therefore, the increase in propene yield after 773 K can be attributed to the dehydrogenation of propane into propene.

Fig. 7(e) illustrates the propane production in the oxidative cracking of *n*-eicosane with oxygen at 1 bar. Both alkanes, ethane and propane, show similar production trends as observed in Fig. 6(g) and Fig. 7(e). The number of moles of propane increases gradually until it reached a maximum point at a range of 700 K–800 K. Then, the yield of propane continues to decrease with the increase in temperature. A higher EO ratio, EO ratio 0.95:0.05 tends to promote propane production due to the higher number of carbons available in the reactant, while lower EO ratio only shows a minor fluctuation on the mole of propane produced under studied parameters. The decomposition of larger hydrocarbons such as butane in the chain reaction leads to the formation of propane.

The 1,3-butadiene production in the oxidative cracking of *n*-eicosane with oxygen at 1 bar is shown in Fig. 7(f). Generally, the trend of alkadiene production is similar to that in alkyne. A higher EO ratio recorded a higher mole of alkadiene. However, the increment of C_4H_6 at equilibrium composition could be found at a lower temperature which is 973 K (Zeng et al., 2018). Production of C_4H_6 before 973 K is almost negligible. As shown in Fig. 8(a), the conversion of butene into C_4H_6 via dehydrogenation and oxidative dehydrogenation occurs. Hence, the number of moles of butene decreases while the number of moles of C_4H_6 increases after 1073 K.

Fig. 7(g) shows the butene production in the oxidative cracking of *n*-eicosane with oxygen at 1 bar. The production of butene at temperature lower than 713 K is almost negligible. The yield of butene increases after 713 K and reaches a maximum yield around 973 K–1073 K. Then, the yield begins to decrease at a higher temperature. Higher EO ratio showed a higher butene production as there is a higher number of carbons in the reactants. The overall production of butene is unappealing at the studied temperature. As illustrated in Fig. 5(a), butene's formation depends on the primary reaction: the oxidative cracking of n-eicosane with oxygen.

3.4. *Pressure and temperature effect on oxidative cracking of n-eicosane with oxygen*

The pressure and temperature effect on oxidative cracking of *n*-eicosane with oxygen for EO ratio 0.95:0.05 was further investigated on the production of hydrogen, methane, carbon, CO, ethane and ethene. This section aims to provide a better view of the reaction parameters that lead to higher production of some major products, particularly hydrogen. It can be found that the total alkane production at equilibrium is higher than the total alkene production at all temperature and pressure. The major products that are formed under different pressure would remain the same. However, pressure could show a significant effect on the selectivity of each product. Higher pressure would restrict the unimolecular reaction but promote bimolecular reaction to occur (Chakraborty and Kunzru, 2009; Liu et al., 2020; Wu et al., 2018). Based on Fig. 8(a), the highest yield of hydrogen is recorded at higher temperature and lower pressure. This is similar to the hydrogen production in a previous study on the cracking of *n*-hexane (Li and Zhao, 2015). Inversely, the production of methane as shown in Fig. 8(b), is more favoured at lower temperature with higher pressure. This is due to the alkane formation via H-abstraction and radical recombination process that favour low temperature and high pressure conditions (Wu et al., 2018; 2019a, 2019b). However, the production of ethane in Fig. 8(f) shows a higher yield in a high pressure but not limited to low temperature. At high pressure, a higher yield of ethane is detected in the range of 873 K–1073 K.

Fig. 8(c) shows the carbon production in the oxidative cracking of n-eicosane with oxygen at different temperature and pressure. Higher pressure and lower temperature hinder the production of carbon as a by-product in the oxidative cracking process. Proper control on the formation of carbon is beneficial as carbon could be utilized in various field.

Fig. 8(d) illustrates the CO production in the oxidative cracking of *n*-eicosane with oxygen at different temperature and pressure. The mole of CO produced is higher at lower pressure with higher temperature. Since the production trend of both hydrogen and CO is similar, the reaction parameter could be controlled at a suitable range for the higher formation of syngas (hydrogen and CO) that has high economic value in petrochemical industries.

The ethylene production in the oxidative cracking of *n*-eicosane with oxygen at different temperature and pressure in shown in Fig. 8(e). Higher temperature and higher pressure promote the production of ethene. This might contrast with the alkene formation theory proposed in pyrolysis process from a previous study, where alkene formation is higher when the temperature increase and pressure decrease (Li and Zhao, 2015). This situation might be explained by the addition of oxygen in the cracking process, leading to other side reactions compared to traditional cracking.

3.5. *Hydrogen to carbon ratio*

The upgrading of a low H/C ratio fuel oil is aimed to produce lighter fuel with a higher H/C ratio. This is because the H/C ratio on fuel will directly impact the amount of carbon dioxide released during combustion. Therefore, it can be said that the higher the H/C ratio, the higher the efficiency of fuel which brings lesser impact to the environment during its burning process. The production of hydrogen in this study could be the opportunity to produce carbon-free energy with zero greenhouse gasses emission to replace the usage of fossil fuels in industries (Abdalla et al., 2018).

The H/C ratio of HFO depends on the compositions of the main components: saturates, aromatics, resins, and asphaltenes. Each component might have different H/C ratios that would affect the cracking performance of the feedstock. When a FOBS with a higher H/C ratio is chosen as the reactant, the liquid products yields could be increased and the formation of coke at equilibrium could be reduced at the same time (Wang et al., 2015). This is because a feedstock with a higher H/C ratio showed a better secondary cracking performance. When the heavy oil is used as the feedstock, the H/C ratio in both resins and asphaltenes of the product formed decrease when a small amount of catalyst is employed (Sviridenko et al., 2020). When SARA analysis is performed, it could be found that the atomic H/C ratio of asphaltenes is lowest while in saturates is highest (Wang et al., 2020). The asphaltenes with higher aromaticity contribute to higher coke in the reactor. Therefore, it

could be observed that coking is more significant in feedstock with a lower H/C ratio.

On the other hand, except for n-alkane model compounds, it was proven that feedstock with a higher H/C ratio produces more gas products than feedstock with a lower H/C ratio (Yue et al., 2016). This is because the H/C ratio of n-alkane decrease when the molecular weight increases. Larger alkane feedstock cracks more easily due to the structural impact. As a result, it could be predicted that the oxidative cracking of *n*-eicosane in this study produces a higher yield of gas products than other alkanes with lower molecular weight (higher H/C ratio).

In the oxidative cracking of *n*-eicosane, the production of carbon is mainly affected by the hydrogen availability at equilibrium. It could be observed that the yield of hydrogen and carbon show a similar production trend, which is increasing under high temperature. The three main types of hydrocarbons that had been formed are alkane, alkene and alkyne. The alkane has the highest H/C, followed by alkene, while the alkyne has the lowest H/C.

Among the products formed, the lighter gas, such as methane, has the highest hydrogen to carbon ratio (H/C) compared to other larger hydrocarbons. The formation of high H/C lighter gas in the oxidative cracking process would promote the production of carbon through R10 that later promotes hydrogen disproportionation reaction (Zachariah et al., 2013). Understanding the H/C ratio could help provide better control on the production of carbon and hydrogen during the oxidative cracking process. The equilibrium favours the production of olefins at high temperatures. When more olefins with lower H/C are produced, the H/C in the remaining products increase. Thus, increasing the possibility of decomposition of a higher H/C product to produce more hydrogen and carbon.

Other than oxidative cracking of FOBS, the addition of hydrogen in the cracking process could also increase the H/C ratio of products formed (Bellussi et al., 2013). As a result, more attractive product distribution is obtained because the feedstock is saturated with the additional hydrogen supplied. Furthermore, as found in previous research, the H/C ratio of liquid products obtained is also affected by the availability of active sites of the catalyst used (Nguyen-Huy and Shin, 2017).

3.6. *Feasibility and future perspective*

The outcomes of this study could accelerate industrial advancement in the upgrading of FOBS. The increasing number of petrochemical refineries worldwide has, with no intention, also increased the production of FOBS. Since the chemical and physical properties of FOBS are unattractive and at the same time the value is low, it could potentially be a good and cheap feedstock to produce higher value-added product. With the right technology and know-how, FOBS can be transformed into hydrogen and precious derivatives. From a different perspective, direct usage of FOBS provide better impact to the environment, such as the release of harmful and toxic particles could be reduced by providing alternative usage of FOBS.

It is well-known that thermal cracking has the lowest costs among the upgrading technologies of FOBS. However, the oxidative cracking could offer better solution. This research provides a simple technology improvisation towards the traditional thermal cracking with low capital investments. Only minor changes are required to deliver ambient air which contains ambient oxygen into the reactor. Therefore, it is economically feasible and able to bring long-term benefits to industries. The amount of oxygen feed to the reactor is controlled wisely to prevent explosion under high oxygen content (Shvets et al., 2017).

Nevertheless, a more significant amount of olefins with higher market demand and lesser paraffins could be formed in an equilibrium composition with the addition of catalyst (Kar et al., 2018). However, it is undeniable that expensive capital investment is needed when a catalyst is employed in the oxidative catalytic cracking of FOBS. This is because the use of catalysts is highly affected by coke formation. The coke deposition on the surface of catalysts restricts access to the pores of the catalyst. The deactivation of catalysts would reduce the efficiency of the working cycle of a fixed-bed reactor. The situation has deteriorated when the feedstock employed contains a high metal concentration, increasing the risk of irreversible deactivation in the catalyst (Gao et al., 2012). As a result, the expenditure on catalytic oxidative cracking increases due to the rise in catalyst consumption to ensure the reactor operates at its optimum condition. Additional investigation is needed to suppress the formation of coke when a catalyst is applied in the cracking process. From a commercial point of view, the use of catalyst in oxidative cracking of FOBS is not favourable as most of the catalyst in the market is expensive. Moreover, the addition of catalyst causes the oxidative cracking process to become more complicated as catalyst characterization is needed to ensure the quality of the catalyst used (Sviridenko et al., 2020). At the same time, more cost is spent and other technologies are required for the preparation of the catalyst. In contrast, oxidative cracking without a catalyst is a more simple, convenient and cost-saving process. Furthermore, the irreversible poisoning solid catalyst left as a scheduled waste in the reactor. Therefore, extra expenditures on the handling and treatment of scheduled waste are needed before disposal. The waste generators also need to provide proper training to the workers in handling the waste. Even though catalysts would produce better product distribution and reduce the operating condition, the long-term effect of oxidative catalytic cracking brings adverse effects to the environment and the investor. Consequently, it is suggested to apply oxidative cracking without the catalyst for long-term benefits.

Experiment work on oxygenated cracking of FOBS is needed to verify the validity of this result. Other simulation software such as Aspen Plus, MATLAB and Chemkin code could be used to better agree on the production trends of the products. Since HFO is a complex compound that is impractical to identify the exact components, other hydrocarbons under the class of saturate and aromatic could also be selected as a surrogate fuel for HFO in future studies.

4. Conclusion

The thermodynamics analysis of oxygenated cracking of FOBS is performed using HSC Chemistry. The precise finding based on simulation could serve as a starting point for controlling this process in industries. Based on the minimization of Gibbs free energy, it was observed that the conversion of FOBS into hydrogen, carbon, methane and carbon monoxide is higher than other light hydrocarbons. A reaction network consisting of all major and minor products is proposed based on the chain mechanism during the process. The numerical results indicated that the optimum condition for hydrogen production is achieved at EO ratio 0.95:0.05, temperature 1273 K at 1

bar, while for hydrocarbon production, methane production is optimum at EO ratio 0.95:0.05, temperature 573 K and 1 bar pressure. In addition, the yield of both hydrogen and carbon monoxide is optimum at higher temperature and lower pressure while methane production shows inverse conditions when both temperature and pressure are considered. The atmospheric pressure operating condition suggested in this research is cost-saving compared to a high-pressure condition that needs extra safety concerns. A more comprehensive experiment to investigate the detailed mechanism can be performed in future to provide a better understanding of the process.

Declaration of interests

The authors declare that they have no known competing financial interests or personal relationships that could have appeared to influence the work reported in this paper.

Acknowledgement

The authors would like to thank Universiti Teknologi Malaysia's Collaborative Research Grant (4B485) and Ministry of Higher Education Malaysia (MOHE) for the financial support through Fundamental Research Grant Scheme (FRGS/1/2020/TK0/UTM/02/97).

References

Abdalla, A.M., Hossain, S., Nisfindy, O.B., Azad, A.T., Dawood, M., Azad, A.K., 2018. Hydrogen production, storage, transportation and key challenges with applications: a review. Energy Convers. Manage. 165, 602–627, http://dx.doi.org/10.1016/j.enconman.2018.03.088.

Agency, E.I., 2021. Heavy Fuel Oil – EIA Global [WWW Document], URL https://eia-global.org/subinitiatives/heavy-fuel-oil-in-the-arctic/.

Akhavan, A., Jabbari, N., Hamdi, M., 2014. A design integrated model in strategy management for upgrading heavy oils. Pet. Sci. Technol. 32, 2845–2852, http://dx.doi.org/10.1080/10916466.2013.858746.

Al-Malack, M.H., Bukhari, A.A., Al-Muhanna, H.H., 2016. Integrated disposal scheme of heavy fuel oil flyash in Saudi Arabia. Arab. J. Sci. Eng. 41, 3911–3921.

Alonso-Ramírez, G., Sánchez-Minero, F., Ramírez, J., Cuevas-Garcia, R., Moreno-Montiel, N., 2018. Analysis of the thermal hydrocracking of heavy fuel oil. Pet. Sci. Technol. 36, 507–513.

Angeles, M.J., Leyva, C., Ancheyta, J., Ramírez, S., 2014. A review of experimental procedures for heavy oil hydrocracking with dispersed catalyst. Catal. Today 220–222, 274–294, http://dx.doi.org/10.1016/j.cattod.2013.08.016.

Bellussi, G., Rispoli, G., Landoni, A., Millini, R., Molinari, D., Montanari, E., Moscotti, D., Pollesel, P., 2013. Hydroconversion of heavy residues in slurry reactors: developments and perspectives. J. Catal. 308, 189–200, http://dx.doi.org/10.1016/j.jcat.2013.07.002.

Boyadjian, C., Lefferts, L., Seshan, K., 2010. Catalytic oxidative cracking of hexane as a route to olefins. Appl. Catal. A Gen. 372, 167–174, http://dx.doi.org/10.1016/j.apcata.2009.10.030.

Chakraborty, J.P., Kunzru, D., 2009. High pressure pyrolysis of n-heptane. J. Anal. Appl. Pyrolysis 86, 44–52, http://dx.doi.org/10.1016/j.jaap.2009.04.001.

Conti, J., Holtberg, P., Diefenderfer, J., LaRose, A., Turnure, J.T., Westfall, L., 2016. International Energy Outlook 2016 with Projections to 2040. USDOE Energy Information Administration (EIA), Washington, DC (United State).

Dante, R.C., Geffroy-Aguilar, E., Chávez, A.E., 2006. Viscoelastic models for Mexican heavy crude oil and comparison with a mixture of heptadecane and eicosane. Part I. Fuel 85, 559–568, http://dx.doi.org/10.1016/j.fuel.2005.08.003.

Dar, H.J., Jakobsen, H.A., Rout, K.R., Jens, K.J., Chen, D., 2021. Autothermal gas-phase oxidative dehydrogenation of ethane to ethylene at atmospheric pressure. Ind. Eng. Chem. Res., http://dx.doi.org/10.1021/acs.iecr.1c00678.

Demirbas, A., Bafail, A., Nizami, A.-S., 2016. Heavy oil upgrading: unlocking the future fuel supply. Pet. Sci. Technol. 34, 303–308, http://dx.doi.org/10.1080/10916466.2015.1136949.

Elordi, G., Olazar, M., Lopez, G., Artetxe, M., Bilbao, J., 2011. Continuous polyolefin cracking on an HZSM-5 zeolite catalyst in a conical spouted bed reactor. Ind. Eng. Chem. Res. 50, 6061–6070.

Eshraghian, A., Husein, M.M., 2018. Catalytic thermal cracking of Athabasca VR in a closed reactor system. Fuel 217, 409–419, http://dx.doi.org/10.1016/j.fuel.2017.12.115.

Gao, H., Wang, G., Wang, H., Chen, J., Xu, C., Gao, J., 2012. A conceptual catalytic cracking process to treat vacuum residue and vacuum gas oil in different reactors. Energy Fuels 26, 1870–1879, http://dx.doi.org/10.1021/ef201815z.

Garaniya, V., McWilliam, D., Goldsworthy, L., 2011. Chemical characterization of heavy fuel oil for combustion modelling, September 2011. In: Conference: Proceedings of the World Engineers Convention 2011 (WEC2011), Geneva, Switzerland.

Ghashghaee, M., 2017. Heterogeneous catalysts for gas-phase conversion of ethylene to higher olefins. Int. Rev. Chem. Eng. 34, http://dx.doi.org/10.1515/revce-2017-0003.

Ghashghaee, M., Shirvani, S., 2018. Two-step thermal cracking of an extra-heavy fuel oil: experimental evaluation, characterization, and kinetics. Ind. Eng. Chem. Res. 57, 7421–7430, http://dx.doi.org/10.1021/acs.iecr.8b00819.

Hart, A., Leeke, G., Greaves, M., Wood, J., 2014. Down-hole heavy crude oil upgrading by CAPRI: effect of hydrogen and methane gases upon upgrading and coke formation. Fuel 119, 226–235, http://dx.doi.org/10.1016/j.fuel.2013.11.048.

Hasanova, A., Alizade, A., Ahmadova, R., Mukhtarova, G., Abbasov, V., 2019. Hydrocracking process of fuel oil using halloysite modified by different methods. Appl. Petrochemical Res. 9, 199–209, http://dx.doi.org/10.1007/s13203-019-00234-7.

He, L., Yang, J., Chen, D., 2013. In: Gandía, L.M., Arzamendi, G., Diéguez, P.M.B.T.-R.H.T. (Eds.), Chapter 6 - Hydrogen from Biomass: Advances in Thermochemical Processes. Elsevier, Amsterdam, pp. 111–133, http://dx.doi.org/10.1016/B978-0-444-56352-1.00006-4.

Henderson, L., Shukla, P., Rudolph, V., Duckworth, G., 2020. Production of cyanide using thermal plasma: thermodynamic analysis and process-specific energy consumption. Ind. Eng. Chem. Res. 59, 21347–21358, http://dx.doi.org/10.1021/acs.iecr.0c02140.

Hosseinpour, M., Hajialirezaei, A.H., Soltani, M., Nathwani, J., 2019. Thermodynamic analysis of in-situ hydrogen from hot compressed water for heavy oil upgrading. Int. J. Hydrogen Energy 44, 27671–27684, http://dx.doi.org/10.1016/j.ijhydene.2019.08.223.

Jiang, H., Zhao, Y., Niu, L., Weng, H., 2013. Molecular reconstruction of crude oil. Pet. Sci. Technol. 31, 1992–2003, http://dx.doi.org/10.1080/10916466.2011.555342.

Jiang, P.-X., Wang, Y., Zhu, Y., 2019. Differential global reaction model with variable stoichiometric coefficients for thermal cracking of n-decane at supercritical pressures. Energy Fuels 33, 7244–7256, http://dx.doi.org/10.1021/acs.energyfuels.9b01505.

Jin, B., Jing, K., Liu, J., Zhang, X., Liu, G., 2017. Pyrolysis and coking of endothermic hydrocarbon fuel in regenerative cooling channel under different pressures. J. Anal. Appl. Pyrolysis 125, 117–126, http://dx.doi.org/10.1016/j.jaap.2017.04.010.

Kar, Y., Göksu, D.Ş., Yalman, Y., 2018. Characterization of light diesel fraction obtained from upgraded heavy oil. Egypt. J. Pet. 27, 1301–1304, http://dx.doi.org/10.1016/j.ejpe.2018.08.001.

Laffon, B., 2014. Fuel oils. In: Wexler, P. (Ed.), Encyclopedia of Toxicology. , third edition. Academic Press, Oxford, pp.

667–670, http://dx.doi.org/10.1016/B978-0-12-386454-3.00024-5.
Lee, S.H., Choi, C.S., 2000. Chemical activation of high sulfur petroleum cokes by alkali metal compounds. Fuel Process. Technol. 64, 141–153, http://dx.doi.org/10.1016/S0378-3820(00)00070-9.
Li, D., Zhao, Y., 2015. Understanding the chain mechanism of radical reactions in n-hexane pyrolysis. Res. Chem. Intermed. 41, 3507–3529, http://dx.doi.org/10.1007/s11164-013-1468-6.
Liu, X., Li, W., Xu, H., Chen, Y., 2004. Production of light alkenes with low CO2 emission from gas phase oxidative cracking (GOC) of hexane. React. Kinet. Catal. Lett. 81, 203–209, http://dx.doi.org/10.1023/B:REAC.0000019424.06619.28.
Liu, P., Zhou, H., Gao, X., Zhu, Q., Wang, J., Li, X., 2016. An experimental and numerical investigation on thermal cracking of n-decane in the microchannel. Pet. Sci. Technol. 34, 555–561, http://dx.doi.org/10.1080/10916466.2016.1149490.
Liu, P., Zhang, T., Zhou, L., Chen, Z., Zhu, Q., Wang, J., Li, X., 2019. Experimental and numerical analysis on flow characteristics and pyrolysis mechanism of hydrocarbon fuel with a novel online hybrid method. Energy Convers. Manage. 198, 111817, http://dx.doi.org/10.1016/j.enconman.2019.111817.
Liu, Y., Gong, S., Wang, H., Wang, L., Zhang, X., Liu, G., 2020. Pyrolysis of C8-C16 hydrocarbons with different molecular structures using high-pressure micro-reactor with GC-MS/FID. J. Anal. Appl. Pyrolysis 149, 104864, http://dx.doi.org/10.1016/j.jaap.2020.104864.
Magomedov, R.N., Nikitin, A.V., Savchenko, V.I., Arutyunov, V.S., 2014. Production of gas mixtures with regulated ratios between ethylene and carbon monoxide by the gas-phase oxidative cracking of light alkanes. Kinet. Catal. 55, 556–565, http://dx.doi.org/10.1134/S0023158414050127.
Manasrah, A.D., 2018. Conversion of Petroleum Coke into Valuable Products using Catalytic and Non-Catalytic Oxy-Cracking Reaction. (Unpublished doctoral thesis). University of Calgary, Calgary, AB, http://dx.doi.org/10.11575/PRISM/31818.
McDermott, W.A.-O.X., Venegas, J.A.-O., Hermans, I.A.-O., ChemSusChem, 2020. Selective oxidative cracking of n-butane to light olefins over hexagonal boron nitride with limited formation of CO(x). ChemSusChem 13 (1), 152–158.
Mehariya, S., Iovine, A., Casella, P., Musmarra, D., Figoli, A., Marino, T., Sharma, N., Molino, A., 2020. Chapter 7 - Fischer–Tropsch synthesis of syngas to liquid hydrocarbons. In: Yousuf, A., Pirozzi, D., Sannino, F. (Eds.), Lignocellulosic Biomass to Liquid Biofuels. Academic Press, pp. 217–248, http://dx.doi.org/10.1016/B978-0-12-815936-1.00007-1.
Nabil, M., Khodadadi, J.M., 2013. Experimental determination of temperature-dependent thermal conductivity of solid eicosane-based nanostructure-enhanced phase change materials. Int. J. Heat Mass Transf. 67, 301–310, http://dx.doi.org/10.1016/j.ijheatmasstransfer.2013.08.010.
Nguyen-Huy, C., Shin, E.W., 2017. Oxidative cracking of vacuum residue with steam over NiK/CeZr–Al catalysts. Fuel 192, 149–157, http://dx.doi.org/10.1016/j.fuel.2016.12.026.
Pei, S., Huang, L., Zhang, L., Ren, S., 2020. Experimental study on thermal cracking reactions of ultra-heavy oils during air injection assisted in-situ upgrading process. J. Pet. Sci. Eng. 195, 107850, http://dx.doi.org/10.1016/j.petrol.2020.107850.
Perry, R.H., Green, D.W., Maloney, J., 1998. Perry's Chemical Engineers' Handbook, 7th intl. ed. McGraw-Hill Education - Europe, New York, United States.
Program, N.T., n.d. Institute of Environmental Health Sciences, National Institutes of Health (NTP). 1992. Natl. Toxicol. Progr. Chem. Repos. Database. Res. Triangle Park. North Carolina NTP via httn.canieochemicals.noaa.gov/chemical/20568.
Roine, A., 1999. HSC chemistry for windows—chemical reaction and equilibrium software with extensive thermochemical database. Outokumpu, HSC Chem. Wind. ReOutokumpu Res. Oy. Pori.
Rueda-Velásquez, R.I., Gray, M.R., 2017. A viscosity-conversion model for thermal cracking of heavy oils. Fuel 197, 82–90, http://dx.doi.org/10.1016/j.fuel.2017.02.020.
Safari, S., Ebrahimynejad, M., Karimzadeh, R., 2019. Vacuum residue upgrading by pyrolysis-catalysis procedure over mesoporous ZSM-5 zeolite. J. Oil Gas Petrochemical Technol. 6, 51–62.
Safari, S., Khoshbin, R., Karimzadeh, R., 2020. Catalytic upgrading of heavy oil over mesoporous HZSM-5 zeolite in the presence of atmospheric oxygen flow. React. Kinet. Mech. Catal. 129, 941–962, http://dx.doi.org/10.1007/s11144-020-01731-w.
Schmidt, P.F., 1985. Fuel Oil Manual. Industrial Press Inc.
Shimada, I., Kobayashi, Y., Ohta, H., Suzuki, K., Takatsuka, T., 2018. Hydrocarbon fuel production from lignocellulosic biomass by solvolysis and catalytic cracking. J. Japan Pet. Inst. 61, 302–310, http://dx.doi.org/10.1627/jpi.61.302.
Shrestha, U., Rahimi, M.J., Simms, G.P., Chelliah, H.K., 2017. Fuel pyrolysis in a microflow tube reactor–measurement and modeling uncertainties of ethane, n-butane, and n-dodecane pyrolysis. Combust. Flame 177, 10–23, http://dx.doi.org/10.1016/j.combustflame.2016.11.019.
Shvets, V., Kozlovskiy, R., Luganskiy, A.I., Gorbunov, A.V., Suchkov, Y.P., Ushin, N.S., Cherepanov, A.A., 2016. Oxygen-induced cracking distillation of oil in the continuous flow tank reactor. Int. J. Environ. Sci. Educ. 11, 4855–4868.
Shvets, V., Sapunov, V.N., Kozlovskiy, R., Luganskiy, A.I., Gorbunov, A.V., Sovetin, F.S., Gartman, T.N., 2017. Cracking of heavy oil residues in a continuous flow reactor, initiated by atmospheric oxygen. Chem. Eng. J. 329, http://dx.doi.org/10.1016/j.cej.2017.05.104.
Stratiev, D., Shishkova, I., Nikolova, R., Tsaneva, T., Mitkova, M., Yordanov, D., 2016. Investigation on precision of determination of SARA analysis of vacuum residual oils from different origin. Pet. Coal 58, 109–119.
Sun, X., Liang, X., Shu, G., Yu, H., Liu, H., 2019. Development of surrogate fuels for heavy fuel oil in marine engine. Energy 185, 961–970, http://dx.doi.org/10.1016/j.energy.2019.07.085.
Sviridenko, N.N., Golovko, A.K., Kirik, N.P., Anshits, A.G., 2020. Upgrading of heavy crude oil by thermal and catalytic cracking in the presence of NiCr/WC catalyst. J. Taiwan Inst. Chem. Eng. 112, 97–105, http://dx.doi.org/10.1016/j.jtice.2020.06.018.
Taghili, N., Manteghian, M., Jafari, A., 2020. Novel preparation of MoO3/γ-Al2O3 nanocatalyst: application in extra-heavy oil visbreaking at atmospheric pressure. Appl. Nanosci. 10, 1603–1613, http://dx.doi.org/10.1007/s13204-020-01271-8.
Wang, K., Zhang, J., Shanks, B.H., Brown, R.C., 2015. Catalytic conversion of carbohydrate-derived oxygenates over HZSM-5 in a tandem micro-reactor system. Green Chem. 17, 557–564.
Wang, B., Duan, P.-G., Xu, Y.-P., Wang, F., Shi, X.-L., Fu, J., Lu, X.-Y., 2017. Co-hydrotreating of algae and used engine oil for the direct production of gasoline and diesel fuels or blending components. Energy 136, 151–162, http://dx.doi.org/10.1016/j.energy.2016.03.084.
Wang, T., Liu, Q., Shi, L., Xiang, C., Liu, Z., Han, W., Zhang, L., Nie, H., Li, M., 2020. Radicals and coking behaviors during thermal cracking of two vacuum resids and their SARA fractions. Fuel 279, 118374, http://dx.doi.org/10.1016/j.fuel.2020.118374.
Wu, Y., Wang, X., Song, Q., Zhao, L., Su, H., Li, H., Zeng, X., Zhao, D., Xu, J., 2018. The effect of temperature and pressure on n-heptane thermal cracking in regenerative cooling channel. Combust. Flame 194, 233–244, http://dx.doi.org/10.1016/j.combustflame.2018.04.036.
Wu, Y., Wang, N., Wang, X., Li, H., Zeng, X., Bai, J., 2019a. Reaction kinetic analysis of the effect of pressure on ethylene selectivity of n-heptane pyrolysis. J. Energy Inst. 92, 144–152, http://dx.doi.org/10.1016/j.joei.2017.10.013.
Yaws, C.L., Gabbula, C., 2003. YawsḦandbook of Thermodynamic and Physical Properties of Chemical Compounds. Knovel.
Yue, L., Li, G., He, G., Guo, Y., Xu, L., Fang, W., 2016. Impacts of hydrogen to carbon ratio (H/C) on fundamental properties and supercritical cracking performance of hydrocarbon fuels. Chem. Eng. J. 283, 1216–1223, http://dx.doi.org/10.1016/j.cej.2015.08.081.
Wu, Z., Mao, Y., Yu, L., Wang, S., Xia, J., Qian, Y., Lu, X., 2019b. Surrogate formulation for marine diesel considering some

important fuel physical–chemical properties. Energy Fuels 33, 3539–3550, http://dx.doi.org/10.1021/acs.energyfuels.8b04253.
Zachariah, A., Wang, L., Yang, S., Prasad, V., de Klerk, A., 2013. Suppression of coke formation during bitumen pyrolysis. Energy Fuels 27, 3061–3070, http://dx.doi.org/10.1021/ef400314m.
Zeng, G., Tian, Y., Li, Y., 2010. Thermodynamic analysis of hydrogen production for fuel cell via oxidative steam reforming of propane. Int. J. Hydrogen Energy 35, 6726–6737, http://dx.doi.org/10.1016/j.ijhydene.2010.03.099.
Zeng, M., Yuan, W., Wang, Y., Zhou, W., Zhang, L., Qi, F., Li, Y., 2014. Experimental and kinetic modeling study of pyrolysis and oxidation of n-decane. Combust. Flame 161, 1701–1715, http://dx.doi.org/10.1016/j.combustflame.2014.01.002.
Zeng, M., Yuan, W., Li, W., Zhang, Y., Wang, Y., 2018. Investigation of n-dodecane pyrolysis at various pressures and the development of a comprehensive combustion model. Energy 155, 152–161, http://dx.doi.org/10.1016/j.energy.2018.04.177.
Zhang, D., Hou, L., Gao, M., Zhang, X., 2018. Experiment and modeling on thermal cracking of n-dodecane at supercritical pressure. Energy Fuels 32, 12426–12434, http://dx.doi.org/10.1021/acs.energyfuels.8b03386.
Zhang, X., Zhu, C., Fang, G., 2020. Preparation and thermal properties of n-eicosane/nano-SiO2/expanded graphite composite phase-change material for thermal energy storage. Mater. Chem. Phys. 240, 122178, http://dx.doi.org/10.1016/j.matchemphys.2019.122178.
Zhao, S., Pu, W., Sun, B., Gu, F., Wang, L., 2019. Comparative evaluation on the thermal behaviors and kinetics of combustion of heavy crude oil and its SARA fractions. Fuel 239, 117–125, http://dx.doi.org/10.1016/j.fuel.2018.11.014.
Zhong, H., Mao, X., Rousso, A.C., Patrick, C.L., Yan, C., Xu, W., Chen, Q., Wysocki, G., Ju, Y., 2021. Kinetic study of plasma-assisted n-dodecane/O2/N2 pyrolysis and oxidation in a nanosecond-pulsed discharge. Proc. Combust. Inst. 38, 6521–6531, http://dx.doi.org/10.1016/j.proci.2020.06.016.
Zhou, P., Hollis, O.L., Crynes, B.L., 1987. Thermolysis of higher molecular weight straight-chain alkanes (C9-C22). Ind. Eng. Chem. Res. 26, 846–852, http://dx.doi.org/10.1021/ie00064a038.
Zhu, H., Liu, X., Ge, Q., Li, W., Xu, H., 2006. Production of lower alkenes and light fuels by gas phase oxidative cracking of heavy hydrocarbons. Fuel Process. Technol. 87, 649–657, http://dx.doi.org/10.1016/j.fuproc.2006.01.009.
Zhu, Y., Liu, B., Jiang, P., 2014. Experimental and numerical investigations on n-decane thermal cracking at supercritical pressures in a vertical tube. Energy Fuels 28, 466–474, http://dx.doi.org/10.1021/ef401924s.